Dalton Transactions

Cite this: *Dalton Trans.*, 2012, **41**, 10430

www.rsc.org/dalton

PAPER

A computational examination on the structure, spin-state energetics and spectroscopic parameters of high-valent Fe^{IV}=NTs species†

Madhavan Jaccob and Gopalan Rajaraman*

Received 17th May 2012, Accepted 13th June 2012
DOI: 10.1039/c2dt31071f

The imidoiron(IV) species are relatively less explored compared to the oxoiron(IV) intermediates. Recently, generation and characterization of a novel imido/oxoiron(IV) species ($[(N_4Py)Fe^{IV}{=}X]^{2+}$ X = NTs; **1**, O; **2**) has been reported with an $S = 1$ ground state. Although the ground state for **1** and **2** are the same, they are reported to be distinctly different in other aspects. Unlike the oxoiron(IV) species, the Fe(IV) and nitrene combination in **1** lead to eight different spin states. Bearing in mind the complexity arising here, we have undertaken a detailed DFT study on this transient intermediate and probed its electronic structure and bonding in comparison to the oxoiron(IV) unit. Our Molecular Orbital, Energy Decomposition Analysis, and Natural Bond Orbital analysis indicates a weaker σ and non-degenerate π* orbitals for **1** in comparison to a stronger σ and degenerate π* orbitals for **2**. The implication of these intricate bonding differences in reactivity is discussed along with the computation of absorption and other spectral parameters. Our results broadly support the proposed $S = 1$ ground state for **1** and provides some useful insight into its electronic structure.

Introduction

Heme and non-heme mononuclear iron enzymes offer selective and effective oxidation of olefins and hydrocarbons which are chemically a challenging process. Oxoiron(IV) species were represented as key reaction intermediates in the catalytic cycles of these enzymes and its functional models.[1–7] Mechanistic aspects of these reactions are widely illustrated by two-state/multi-state reactivity concept.[3,8–23] High electron-donating capability of axial ligands increase the possibility of the participation of the several low-lying excited spin states in the rate-determining step of the reaction.[9–15] The electronic reasons behind the spin-state dependent reactivity were rationalised using exchange-enhanced reactivity (EER) concept and this has been successfully used to rationalise the reactivity pattern of several such complexes.[24–27] These intriguing concepts were illustrated in detail in the oxo-transfer and C–H activation reactions involving oxoiron(IV) species[6,12,24,26,28–44] but very little is known for the analogous imidoiron(IV) species. In a series of seminal non-heme oxygenase biomimetic complexes mediated oxidation of aromatic compounds,[1–3,9,17,21,34,40,45–51] Jensen *et al.*[52] reported the first non-heme tosylimidoiron(IV) complex which is capable of aminating the aromatic compounds efficiently through the nitrene transfer reaction. DFT studies on aliphatic C–H bond amidation and aziridination reactions by P450 and model complexes clearly shows that not only axial ligands to iron but also the substituent on the nitrene nitrogen were found to play a crucial role in deciding the reactivity.[53] Subsequently, a significant number of research groups have reported the synthetic and catalytic applications of monomeric Fe(III)-imido complexes with different types of ligands such as a bulky pyrazolyl/bisphosphionoborate, triazacyclononane, β-diketiminato and bisphosphine.[54–58] These Fe(III)-imido complexes have exceedingly good catalytic potential in the hydrogen atom transfer reactions leading to the formation of the respective amido complexes. Borovik *et al.*[59] reported trigonal-bipyramidal Fe(III) amido complexes with ureate/amidate tripodal ligands that inherit a hydrogen bonding (H-bond) network around the Fe(III)–N unit. Recently Holland and co-workers[60] studied the mechanistic aspects of hydrogen atom transfer (HAT) reactions of a four-coordinated imido complex ($L^{Me}Fe{=}NAd(^tBupy)$) LMeFeNAd (L^{Me} = bulky β-diketiminate ligand, 2,4-bis(2,6-diisopropylphenylimido)pentyl; Ad = 1-adamantyl; *t*Bupy = *tert*-butylpyridine).

Klinker *et al.*[61] studied the formation and relative oxidative abilities of $[(N_4Py)Fe^{IV}{=}NTs]^{2+}$ (N_4Py = *N*,*N*-bis(2-pyridylmethyl)-*N*-bis(2-pyridyl)methylamine) (**1**) and $[(N_4Py)Fe^{IV}{=}O]^{2+}$ (**2**)[62] using experimental and spectroscopic methods. Some preliminary theoretical study has also been undertaken to gain insight into the bonding aspects of complex **1**. A triplet state has been proposed as the ground state for **1** based on applied-field Mössbauer spectroscopy where the measured $A_\perp$ hyperfine tensor value is found to best fit the $S = 1$ state and this is lieu to $A_\perp$ reported for other high-valent iron(IV)-oxo complexes having a triplet spin ground state.[7,10] On the other hand, the possibility of an $S = 2$ ground state is ruled out based on a severely underestimated $A_\perp$ value obtained from the fit.

Department of Chemistry, Indian Institute of Technology Bombay, Powai, Mumbai 400076, India. E-mail: rajaraman@chem.iitb.ac.in; Fax: (+91)22 2576 7152

†Electronic supplementary information (ESI) available. See DOI: 10.1039/c2dt31071f

In spite of high reactivity pattern observed for the high-valent iron(IV) imido complexes, as of now, there is no comprehensive study on the energetics of formation of imidoiron(IV) complexes[63] and their bonding aspects compared to the well characterized oxoiron(IV) intermediates.[64–67] The bare nitrenes are characterized to possess two spin states on its own; singlet having a pair of electron in its p-orbital and a triplet where two electrons are unpaired.[68,69] Electron paramagnetic resonance studies have shown that triplet is the ground state for a number of reported nitrene compounds.[69] Additionally the estimated gap between the triplet–singlet states in nitrenes is relatively small (~18 kJ mol^{-1} for phenylnitrene).[69–71] Besides, nitrenes upon coordination with a metal complex, evolve a complex electronic/spin structure. For copper–nitrene complexes a triplet and singlet state are computed using density functional methods and these states are found to be nearly degenerate.[72,73] For **1**, a complex set of spin states are expected to emerge, considering the fact that the Fe(IV) unit can have $S = 0$, 1 and 2 states with nitrenes having $S = 0$ or 1 states. In the case of species **2**, only $S = 0$, 1 and 2 states due to the Fe(IV)═O moiety is possible with the participation of a low-lying first excited spin state in the reactivity in these species *en route* to the concept of two-state reactivity.[3,18,19,38] Thus it is apparent that addressing the individual spin states are of prime importance in understanding the spectroscopic data accumulated and also to gain understanding on the mechanism of the catalytic reactions.[21,23,27,35,47,74] With this background, here we employ density functional methods to: (i) compute the formation energies of **1** compared to **2** to ascertain the relative stability of formation between these two species, (ii) undertake a limited method assessment based on density functional methods to test both hybrid and non-hybrid functionals on computing the spin-state energetics of **1** (iii) investigate the structure and nature of bonding in **1** and **2** using various theoretical tools such as MO (molecular orbital), NBO (natural bond orbital)[75] and EDA (energy decomposition analysis),[76–78] and (iv) compute the absorption spectra and other spin-Hamiltonian parameters and other spectral features to gain in-depth understanding on the electronic structure of **1** to establish its oxidative ability compared to species **2**.

Formation energetics of 1 and 2

Energetics of formation of these transient species holds the key to their observed reactivity pattern, although there are kinetic requirements to the formation energetics, thermodynamic stability/instability hinders/helps its reactivity with the substrates. Thus, we have decided to compute the energetics of formation for species **1** and **2** for comparison. Experimentally high-valent iron(IV) imido/oxo complexes are generated by the reaction of $Fe^{II}(N_4Py)(NCMe)$ complex with the nitrene/oxygen source (mesityl-*N*-tosylimidoiodinane (MsINTs)/iodosylbenzene (PhIO) according to eqn (1):

$$[Fe^{II}(N_4Py)(NCMe)]^{2+} + PhIX \rightarrow [(N_4Py)Fe^{IV}{=}X]^{2+} + PhI + MeCN \quad (X = NTs\ \mathbf{1}, O, \mathbf{2}) \qquad (1)$$

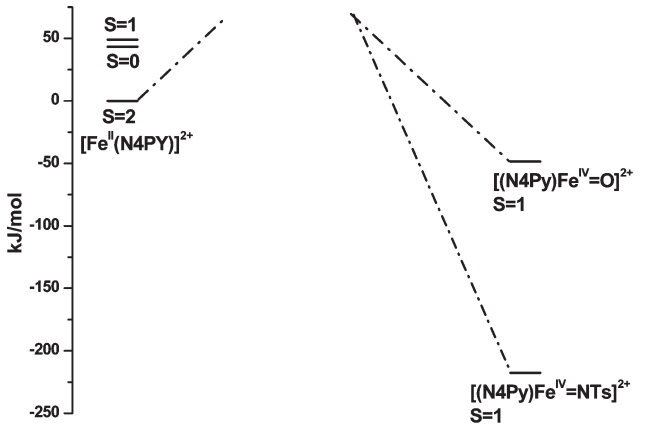

Fig. 1 Potential energy landscape computed for the formation of Fe^{IV}═O *vs.* Fe^{IV}═NTs species from the $[Fe^{II}(N_4Py)]^{2+}$ precursor.

Based on the experimental reports,[72,73] the formation of Fe(IV)–nitrene has been computed from its precursor complex. The calculated free energy of formation of high-valent iron imido complexes is thermodynamically favoured by −217.7 kJ mol^{-1}. To locate the kinetic barrier height that might be involved in the N–I cleavage, a relaxed scan by varying the N–I distances were performed and the results reveal no significant barrier height in the N–I cleavage (see ESI† for a detailed discussion). The formation of species **2** is thermodynamically less favourable (−48.4 kJ mol^{-1}) compared to **1** by 169.1 kJ mol^{-1} (see Fig. 1). The formation energies of species **2** is found to be comparable with the earlier reports on the formation energy of CpdI and PhI from heme and PhIO (−76.3 kJ mol^{-1}).[63,67] A larger thermodynamic drive and no significant kinetic barrier involved in the formation of species **1** is consistent with the experimental report of faster transfer of NTs group from PhINTs in **1** compared to that of the oxo transfer from PhIO in **2** as reported experimentally.[52]

Method assessment and spin-state energetics of $[(N_4Py)Fe^{IV}{=}NTs]^{2+}$

Ground-state properties of **1** were calculated considering all the possible spin states of iron and nitrene electrons. For **1**, there are eight different spin state arising due to the variation in the spin state of Fe^{IV} from $S = 0$, 1 and 2 with nitrene having $S = 0$ and 1 combinations. Additionally, considering the possibility of orthogonality between the two sets of orbitals bearing the unpaired electrons, one can have spin-up and spin-down states with the nitrenes and this resembles the spin states arising due to the spin coupling. The expected spin states for **1** are schematized in Scheme 1.

These states are represented by the following notation $^{M}\mathbf{1}_{(sFe,sN)}$ where superscript 'M' denotes the total multiplicities of the complexes and subscript '$_{(sFe,sN)}$' denotes the spin multiplicity on Fe and N atoms. Among eight different spin states, there are three triplets ($^{3}\mathbf{1}_{(HS,T)}$, $^{3}\mathbf{1}_{(LS,T)}$ $^{3}\mathbf{1}_{(IS,S)}$), two quintets ($^{5}\mathbf{1}_{(IS,T)}$, $^{5}\mathbf{1}_{(HS,S)}$), two singlets ($^{1}\mathbf{1}_{(IS,T)}$, $^{1}\mathbf{1}_{(LS,S)}$) and one heptet state ($^{7}\mathbf{1}_{(HS,T)}$). In order to compute the relative energies of the electronically different spin states of the high-valent Fe^{IV}═NTs complex, we tested four different functionals BP86,[79–81]

B3LYP*,[82,83] and B3LYP[82,83] and M06-2X[84] where the HF exchange correlation is also found to differ by 0, 15, 20 and 54%, respectively. Our aim is to choose the best functional which is capable of predicting the correct ground state for **1**. Table 1 lists the notable geometrical parameters, Mulliken spin densities and relative energies of various spin states of **1** which were obtained from the four different functionals listed above.

Among the four functionals tested, both B3LYP and B3LYP* functionals predict a triplet spin ground state. However, the B3LYP* predicts the $^{7}\mathbf{1}_{(HS,T)}$ state to be extremely high in energy while its corresponding broken symmetry state ($^{3}\mathbf{1}_{(HS,T)}$) to be *ca.* 350 kJ mol^{-1} lower in energy. This situation is very unlikely considering spin-coupling phenomenon which is generally weak in nature.[73] Interestingly, the spin states $^{3}\mathbf{1}_{(LS,T)}$ and $^{3}\mathbf{1}_{(IS,S)}$ have the same energy at this level. Even though these two states are electronically different (see Scheme 1 for the expected electronic configuration), our B3LYP results suggests that these two electronic states are degenerate and the likely reason for this behaviour is a strong π interaction between the d_{xz} and d_{yz} orbitals of Fe with p_x and p_y-type orbitals of the nitrene moiety. This strong π interaction leads to a delocalization of unpaired spins resulting in a near equal distribution of spin densities on both Fe and N atoms for both the triplet states (see Scheme 1). The spin density plot (Fig. 2) of both $^{3}\mathbf{1}_{(LS,T)}$ and $^{3}\mathbf{1}_{(IS,S)}$ states clearly indicates that the two unpaired electrons are strongly delocalized on the nitrene nitrogen and iron centres as well as the oxygen atoms of the tosylate group.

	Electronic Configuration
S=3	$\delta^{\uparrow}\pi^{*\uparrow}_{xz}\pi^{*\uparrow}_{yz}\sigma^{*\uparrow}\delta$ $\varphi_{N1}^{\uparrow}\varphi_{N2}^{\uparrow}$
S=1	$\delta^{\uparrow}\pi^{*\uparrow}_{xz}\pi^{*\uparrow}_{yz}\sigma^{*\uparrow}\delta$ $\varphi_{N1}^{\downarrow}\varphi_{N2}^{\downarrow}$
S=2	$\delta^{\uparrow\downarrow}\pi^{*\uparrow}_{xz}\pi^{*\uparrow}_{yz}\sigma^{*}\delta$ $\varphi_{N1}^{\uparrow}\varphi_{N2}^{\uparrow}$
S=0	$\delta^{\uparrow\downarrow}\pi^{*\uparrow}_{xz}\pi^{*\uparrow}_{yz}\sigma^{*}\delta$ $\varphi_{N1}^{\downarrow}\varphi_{N2}^{\downarrow}$
S=1	$\delta^{\uparrow\downarrow}\pi^{*\uparrow\downarrow}_{xz}\pi^{*}_{yz}\sigma^{*}\delta$ $\varphi_{N1}^{\uparrow}\varphi_{N2}^{\uparrow}$
S=2	$\delta^{\uparrow}\pi^{*\uparrow}_{xz}\pi^{*\uparrow}_{yz}\sigma^{*\uparrow}\delta$ $\varphi_{N1}^{\uparrow\downarrow}\varphi_{N2}$
S=1	$\delta^{\uparrow\downarrow}\pi^{*\uparrow}_{xz}\pi^{*\uparrow}_{yz}\sigma^{*}\delta$ $\varphi_{N1}^{\uparrow\downarrow}\varphi_{N2}$
S=0	$\delta^{\uparrow\downarrow}\pi^{*\uparrow\downarrow}_{xz}\pi^{*}_{yz}\sigma^{*}\delta$ $\varphi_{N1}^{\uparrow\downarrow}\varphi_{N2}$

Scheme 1 All the possible spin configurations arising from the combination of electrons of iron and nitrogen centres.

The degree of spin distribution is found to vary among the functional employed; with B3LYP and B3LYP* providing a similar picture and BP86 and MO6-2X yielding diverse amount of spin densities on Fe and N atoms. Due to this difference, these states are predicted to be non-degenerate by BP86 and MO6-2X functionals. Similarly at B3LYP level, the electronic states $^{5}\mathbf{1}_{(IS,T)}$ and $^{5}\mathbf{1}_{(HS,S)}$ are found to be degenerate and these states also yield similar spin densities distribution on Fe and N atoms. With BP86 functional, the ground spin state is a triplet state with a $^{3}\mathbf{1}_{(LS,T)}$ configuration. The spin state energetics obtained from the M06-2X functional is very different from the other functionals and this functional is found to provide a more localized description, as a significant enhancement in the magnitude of spin densities on the Fe and N atoms are observed.[85,86] The M06-2X functional predicts the $^{7}\mathbf{1}_{(HS,T)}$ state to be the ground state and this is in contrast to the experimental results and the results obtained from other functionals. Optimized structures reveal that the spin states $^{3}\mathbf{1}_{(LS,T)}$ and $^{3}\mathbf{1}_{(IS,S)}$, have the same Fe–N bond distance of 1.76 Å and this structural parameter is in good agreement with the EXAFS fitting measured bond distance of 1.73 Å.[61] Table 2 lists the optimized geometrical parameters obtained from B3LYP and M06-2X functionals. From these structural parameters, it is apparent that the states with high-spin configuration on Fe have longer Fe–N distances while states with low-spin Fe-configuration have shorter Fe–N distances. It is to be noted here that, for $^{3}\mathbf{1}_{(IS,S)}$ spin state having $(d_{xy})^2(d_{xz})^1(d_{yz})^1(d_{z^2})^0(d_{x^2-y^2})^0$ Fe configuration, the d_{z^2} and $d_{x^2-y^2}$ orbitals are found to be close lying (0.36 eV) and in high-spin configuration; filling these orbitals lead to a Jahn–Teller like distortion leading to a significant difference between axial and equatorial bond distances. The Fe–N bond distances computed at M06-2X level were found to be in general longer than those obtained from B3LYP level as expected from the localized description offered by this functional. Comparing the structure, energetics and spin density distribution and considering the accuracy of the B3LYP functional established earlier,[85] we

Table 1 Relative free energies and Mulliken spin densities of several spin states of **1** at four different functionals with TZVP basis set

	BP86 (0% HF exchange)			B3LYP* (15% HF exchange)			B3LYP (20% HF exchange)			MO6-2X (54% HF exchange)		
$^{M}\mathbf{1}_{(Fe,N)}$	ΔE^{a}	S(Fe)	S(N)	ΔE^{a}	S(Fe)	S(N)	ΔE^{a}	S(Fe)	S(N)	ΔE^{a}	S(Fe)	S(N)
$^{7}\mathbf{1}_{(HS,T)}$	196.3	4.13	1.0	402.1	4.16	1.11	31.3	4.19	1.12	0.0	4.38	1.08
$^{3}\mathbf{1}_{(HS,T)}$	226.4	3.05	−1.1	55.2	2.88	−0.90	48.3	2.94	−0.95	80.1	3.68	−1.76
$^{5}\mathbf{1}_{(IS,T)}$	109.8	2.99	0.63	17.9	2.95	0.74	20.4	2.97	0.76	76.6	2.95	0.91
$^{1}\mathbf{1}_{(IS,T)}$	67.3	0.99	−0.79	30.3	0.91	−0.72	29.6	0.99	−0.79	121.9	1.13	−1.0
$^{3}\mathbf{1}_{(LS,T)}$	0.0	1.11	0.8	0.0	1.05	0.90	0.002	1.04	0.91	136.8	0.98	1.0
$^{5}\mathbf{1}_{(HS,S)}$	149.9	3.87	−0.36	16.9	2.96	0.75	20.4	2.97	0.76	193.3	3.09	1.1
$^{3}\mathbf{1}_{(IS,S)}$	39	1.21	0.73	0.0	1.05	0.90	0.0	1.04	0.93	122.6	1.01	0.97
$^{1}\mathbf{1}_{(LS,S)}$	49.9	0	0	36.9	0	0	59.1	0	0	227.7	0	0

[a] Relative energies including ZPC with respect to the lowest energy configuration are given in kJ mol^{-1}; S(Fe) and S(N) correspond to Mulliken spin densities.

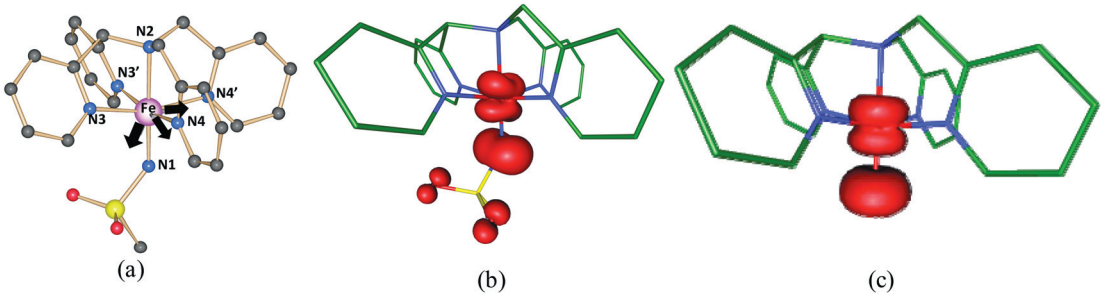

Fig. 2 (a) Optimized geometry of $^{3}\mathbf{1}_{(IS,S)}$ and spin density plots of species (b) **1** and (c) **2**.

Table 2 Optimized geometrical parameters of eight different electronic spin states obtained from B3LYP level (values in parenthesis obtained from M06-2X level). Bond lengths are given in Å and bond angles are given in degrees

$^{M}\mathbf{1}_{(Fe,N)}$	Fe–N1	Fe–N2	Fe–N3	Fe–N3′	Fe–N4	Fe–N4′	N2–Fe–N1
$^{7}\mathbf{1}_{(HS,T)}$	1.97 (2.0)	2.26 (2.24)	2.15 (2.14)	2.21 (2.10)	2.15 (2.13)	2.21 (2.19)	178.3 (168.9)
$^{3}\mathbf{1}_{(HS,T)}$	1.86 (2.15)	2.09 (2.18)	2.16 (2.14)	2.10 (2.19)	2.16 (2.25)	2.19 (2.17)	170.0 (170.3)
$^{5}\mathbf{1}_{(IS,T)}$	1.77 (1.87)	2.09 (2.08)	2.03 (2.02)	2.19 (2.20)	2.32 (2.28)	2.05 (2.03)	176.4 (171.3)
$^{1}\mathbf{1}_{(IS,T)}$	1.82 (1.88)	2.05 (2.06)	1.99 (1.99)	2.02 (2.03)	2.06 (2.09)	2.01 (2.01)	172.1 (170.6)
$^{3}\mathbf{1}_{(LS,T)}$	1.76 (1.87)	2.05 (2.04)	1.99 (2.03)	2.01 (1.99)	2.04 (2.01)	2.01 (2.05)	175.6 (171.1)
$^{5}\mathbf{1}_{(HS,S)}$	1.77 (1.87)	2.09 (2.23)	2.19 (2.13)	2.03 (2.13)	2.05 (2.16)	2.32 (2.16)	176.59 (177.0)
$^{3}\mathbf{1}_{(IS,S)}$	1.76 (1.87)	2.05 (2.04)	1.99 (1.99)	2.04 (2.03)	2.04 (2.00)	2.01 (2.01)	175.6 (171.1)
$^{1}\mathbf{1}_{(LS,S)}$	1.72 (1.71)	2.08 (2.07)	2.02 (1.98)	2.02 (2.04)	2.04 (2.08)	2.04 (2.02)	174.4 (170.9)

conclude that the B3LYP functional behaves marginally better compared to others.

Bonding aspects of $[(N_4Py)Fe^{IV}{=}NTs]^{2+}$ and $[(N_4Py)Fe^{IV}{=}O]^{2+}$

In this section, we are trying to emphasise the bonding nature of **1** compared to **2** with a view to understand the strength of σ and π-bonding and antibonding characters of the Fe=X (X = O, NTs) bond. The ground state electronic configuration of **2** is found to be $(d_{xy})^2(\pi_{d_{xz}-p_x}{}^*)^1(\pi_{d_{yz}-p_y}{}^*)^1(d_{x^2-y^2})^0(d_{z^2}{}^*)^0$ and possesses a short Fe^{IV}–O bond distance (1.62 Å). The key σ- and π-bonding and antibonding orbitals of species **2** are presented in Fig. 3 (left). Two nearly degenerate Fe–O π-antibonding orbitals are formed from the strong overlap between the d_{xz} and the d_{yz} orbitals of Fe and the p_y and p_x orbitals of oxygen. Even though species **1** and **2** possesses a similar electronic configuration, the corresponding Fe–X bond length in **1** is longer than **2** (1.76 *vs.* 1.62 Å).

The computed Fe–X bond lengths for **1** and **2** are different, however it is to be noted here that while species **2** has only an oxo group bound to Fe atom, species **1** has an additional tosylate binding to the nitrogen atom. The Fe–O bond length in a recently reported Fe(IV)=O···Sc^{3+} complex is similar to that found in species **2** (1.75 *vs.* 1.76 Å).[87,88] Additionally the interaction of Sc^{3+} with the Fe(IV)=O is reported to increase the reactivity in oxo transfer and H-atom abstraction reaction compared to the bare Fe(IV)=O complexes. From these arguments one can infer that a longer Fe–X bond enhances the reactivity as this essentially increases the electron density on the oxyl/imido group.[89] A large thermodynamic gain in the formation energetics, and a longer Fe–N distance along with a large spin density (see below) on the nitrogen atom compared to its oxo-counterpart reveals that species **1** is likely to be more reactive than **2** and this is reflected in the experimentally measured half-life period. The degeneracy of two Fe–N π-antibonding orbitals $\pi_{d_{xz}-p_x}{}^*$ and $\pi_{d_{yz}-p_y}{}^*$ are strongly perturbed in **1** (Fig. 3). The splitting of the axial e_g-like orbitals in **1** is also much higher than that of the **2**. All this suggests that the bonding pattern of **1** and **2** are different and this is due to the associated structural and electronic differences.

The spin density on the Fe atom of species **1** is not only delocalized on the nitrogen atom but also on the oxygen atoms of the tosylate groups (ρFe = 0.88; ρN = 0.98; ρO = 0.1; ρO = 0.09). A spin density plot of **1** (Fig. 2b) indicates that a large contribution to the spin densities arise from $\pi_{d_{xz}-p_x}{}^*$ orbitals as the π* orbitals are non-degenerate. On the other hand for **2**, the spin density on the Fe atom is found to be delocalized only on the oxygen atom (ρFe = 1.21; ρO = 0.86) and its spin density plot indicates that the unpaired electron on Fe has equal contributions from the $\pi_{d_{xz}-p_x}{}^*$ and $\pi_{d_{yz}-p_y}{}^*$ orbitals and thus has a dumbbell shape. Besides the nitrene nitrogen has significantly larger spin density and this can eventually promote a facile reaction with the substrates.

For **2**, the σ-antibonding interaction between the Fe–d_{z^2} orbital and O–p_z orbital is found to be much stronger (see Fig. 3) than that of **1**. Further for **2**, the two Fe–O π-antibonding orbitals $\pi(d_{xz}–O–p_x)^*$ and $\pi(d_{yz}–O–p_y)^*$ are nearly degenerate while the two Fe–N π-antibonding orbitals $\pi(d_{xz}–O–p_x)^*$ and $\pi(d_{yz}–O–p_y)^*$ in **1** are non-degenerate in nature and their levels are perturbed by 0.48 eV. Besides, the d_{z^2} orbital in **1** is stabilized to a great extent compared to that of **2**. Additionally, the computed harmonic vibrations for the Fe=X stretching and its corresponding force constant for **1** and **2** reveal distinct differences in the Fe=X strength between these two species. The calculated Fe=N double bond stretch is 726.6 cm^{-1} while Fe=O double

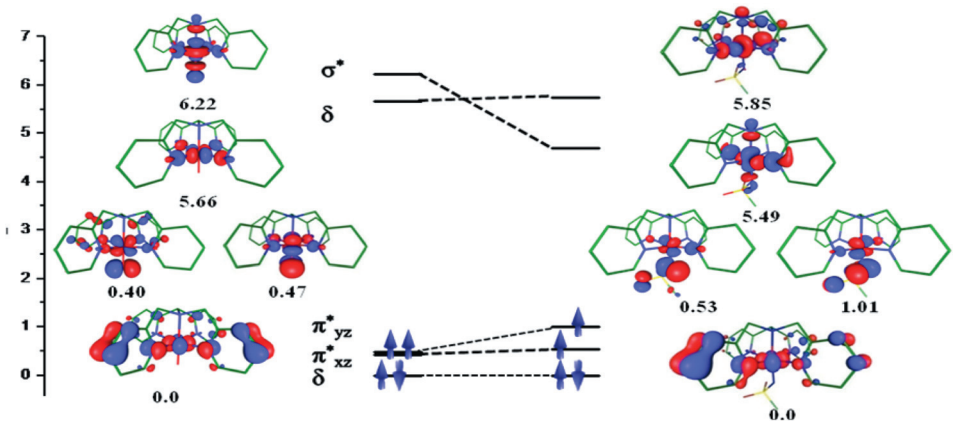

Fig. 3 B3LYP computed high-lying occupied and low-lying unoccupied orbitals of $^{3}\mathbf{1}_{(IS,S)}$ and $^{3}\mathbf{2}_{(IS,S)}$. The relative energies (eV) are scaled from the lowest lying orbitals in each case.

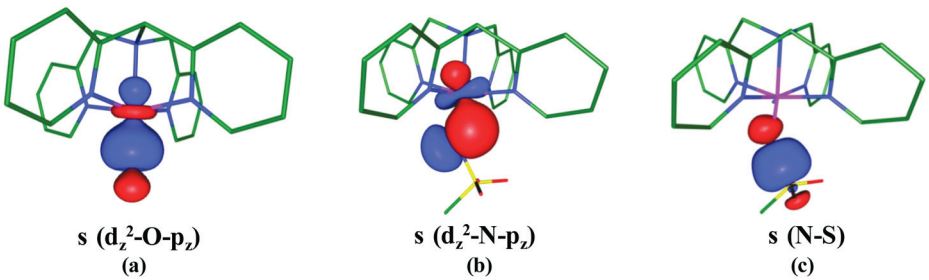

Fig. 4 NBO computed σ-bonding orbitals corresponding to Fe═O (a) and Fe═NTs (b) and N–S interaction (c) in $^{3}\mathbf{1}_{(IS,S)}$ and $^{3}\mathbf{2}_{(IS,S)}$.

bond stretch is found at 947.1 cm^{-1} and the corresponding force constants are 2.13 and 2.86 mdyn $Å^{-1}$ for **1** and **2**, respectively.[115] This estimates also indicates that the Fe═O bond in **2** is stronger than that of the Fe═NTs double bond in **1**.[65]

A detailed NBO analysis has been undertaken to capture the bonding scenario in **1** and **2**. NBO analysis reveals that the σ-bonding interaction in **2** is composed of a Fe(d_{z^2})–O(p_z) orbital (see Fig. 4) while in **1** it is between Fe(d_{z^2})–N(p_y) as the N–p_z orbital is involved in a strong σ-bonding interaction with the sulfur p_z orbital. As the N(p_y) orbital is not along the N2–Fe (see Fig. 1 for labels) axis, the overlap is less significant compared to **2** and it has been noted that the Fe(d_{z^2}) also deviates slightly from the N2–Fe axis to overlap effectively with the N(p_y) orbital. Since this bonding interaction is weak, the corresponding antibonding orbital is less destabilized compared to **1**. This leads to the change in the ordering between d_{z^2} and $d_{x^2-y^2}$ orbitals in the species **1**. The energies of δ character $d_{x^2-y^2}$ orbitals are nearly equal in both the species (see Fig. 3). A less significant but non-negligible Fe(d_{z^2})–σ(N(p_z)–S(p_z) interaction is also detected in the NBO analysis.

Besides, the NBO analysis reveals that the Fe═O σ-bond is composed of 37.3% of Fe–d_{z^2} and 62.7% of O(p_z) orbitals while the Fe═NTs σ-bond is found to have 45.4% of contribution from the Fe(d_{z^2}) orbital and the remainder from the N(p_y) orbital. Further, the donor–acceptor interaction energies obtained from NBO second-order perturbation method allow us to quantify the nature of the Fe═X bond in **1** and **2**. For species **2**, the σ*(Fe(d_{z^2}) → O(p_z)) interaction energy is 625.1 kJ mol^{-1} which is almost twice as large as that of corresponding interaction in **1** (305 kJ mol^{-1}; σ*(Fe(d_{z^2}) → N(p_z)). Since the N(p_y) orbital is also involved in the σ-bonding interactions, the energy of π(Fe-(d_{yz}) –N(p_y))* is significantly lower than π(d_{xz})–N(p_x)* orbital.

To quantify the Fe═X (X = O, NTs) bonding nature in terms of covalent and ionic contributions, we have also performed energy decomposition analysis (EDA)[76–78] on the ground states of **1** and **2** for the comparison at BP86/TZ2P level using ADF[90] suite of programs. The interaction energy of the two fragments is generally represented by three important components (eqn (2)).

$$\Delta E_{int} = \Delta E_{elstat} + \Delta E_{Pauli} + \Delta E_{orb} \quad (2)$$

ΔE_{elstat} gives the electrostatic interaction energy between the fragments, which is calculated with the frozen electron-density distribution in the geometry of the complex. This can be used as an estimate of the electrostatic contribution to the bonding interactions. The second term in the above equation, ΔE_{Pauli}, gives the repulsive orbital interaction between occupied orbitals of the two fragments due to antisymmetrisation. The last term gives the stabilizing orbital interactions, ΔE_{orb}, which can be considered to be an estimate of the covalent contribution to the bonding.[77,91–93] Since the ligand environment is similar in both the complexes, the interaction energy can help to analyse the difference in interaction between O and NTs units with the {LFe^{IV}} unit. The EDA calculations were performed by treating N_4Py, Fe and X (where X = O, NTs) as separate fragments

Table 3 Energy Decomposition Analysis (EDA) of $[Fe^{IV}(X)(N_4Py)]^{2+}$ on $^3\mathbf{1}_{(IS,S)}$ and $^3\mathbf{2}_{(IS,S)}$ (where X = O, NTs). ΔE in kJ mol^{-1}

		{$N_4Py + Fe^{IV} + X$}
$[Fe^{IV}(NTs)(N_4Py)]^{2+}$	ΔE_{int}	−11187.8
	ΔE_{Pauli}	2192.1
	ΔE_{elstat}	−6490.8 (48.5%)
	ΔE_{orb}	−6889.2 (51.5%)
$[Fe^{IV}(O)(N_4Py)]^{2+}$	ΔE_{int}	−10070.6
	ΔE_{Pauli}	3033.9
	ΔE_{elstat}	−8826.9 (67.4%)
	ΔE_{orb}	−4277.6 (32.6%)

(N_4Py + Fe + X). A larger interaction energy and a smaller Pauli repulsion term has been noted for the Fe(IV)–nitrene compared to the Fe(IV)-oxo complex (Table 3). Although the ΔE_{int} and ΔE_{orb} are much larger for **1**, there is a tremendous rise in the ΔE_{elstat} in **2**, revealing again a stronger Fe–O bond. A large difference in the ΔE_{elstat} stems from the electronegativity differences between the two donor atoms. A large ΔE_{elstat} indicates that the bond in **2** is much more ionic in character than **1** – a statement previously verified by the NBO analysis. To this end, we have also computed the $\Delta E_{elstat}/\Delta E_{orb}$ ratio which reveal about the nature of the coordination bond and this ratio is found to be 0.94 and 2.06 for **1** and **2**, respectively, and this reassures that the coordination bonds are much more covalent in **1** than in **2** (Table 3).

The bonding and reactivity can be regarded as two sides of a coin, as a slight perturbation in the bonding can influence the reactivity in great detail. The relevance of bonding of oxoiron(IV) in reactivity is documented in detail elsewhere.[10,64,65,94,95] Here, we compare and contrast the reactivity expected based on the bonding features observed between species **1** and **2**. It has been demonstrated that the triplet–quintet gap is of utmost important in determining the reactivity of non-heme oxoiron(IV) species and at many instances it has been proposed that the molecules having quintet state would enhance the reactivity. In general, for many non-heme oxoiron(IV) systems the barrier height in the quintet transitions surface is smaller than that of the ground-state triplet (two-state reactivity, TSR).[3,17,18,24,25,27,38] One of the main reason for the reduction in barrier height in the quintet surface is the exchange stabilization among the unpaired electrons in the d-block. Although many spin states has been computed for **1**, here we have taken the $^5\mathbf{1}_{(HS,S)}$ to facilitate a direct comparison between **1** and **2**. The energy gap between the ground state and the $^5\mathbf{1}_{(HS,S)}$ is 20.4 kJ mol^{-1} for **1** and this is similar to the triplet–quintet gap of 19.1 kJ mol^{-1} computed for **2**.[10] However for **1** within 30 kJ mol^{-1} of energy window, there are five spin states available including a heptet state which has larger exchange stabilization and this is likely to facilitate a faster reaction compared to **2**, and this is in agreement to the observed reactivity.[52,54,55,61,96,97] As the substrate approaches the nitrene nitrogen atom, initially an electron from the substrate is expected to be transferred to the d-orbital of the Fe and spin-up electron gets transferred in the quintet surface. Analysing the wave function of the quintet state ($^5\mathbf{1}_{(HS,S)}$) reveals that the electronic configuration here is $(d_{xy})^1(\pi_{d_{xz}-p_x}{}^*)^1(\pi_{d_{yz}-p_y}{}^*)^1(d_{z^2})^1$-$(d_{x^2-y^2})^0$ and this demands participation of $(d_{x^2-y^2})$ in the reaction. Our analysis predicts that if an S = 3 ground state iron–nitrene to be synthesised, its reactivity will be much higher than the corresponding oxo complexes.

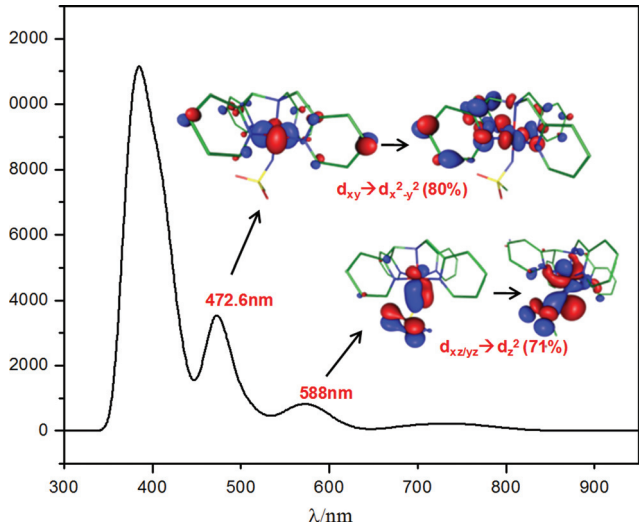

Fig. 5 B3LYP–TDDFT simulated electronic absorption spectra of $^3\mathbf{1}_{(IS,S)}$.

Spectroscopic properties of $[(N_4Py)Fe^{IV}{=}NTs]^{2+}$

To gain further insight into the electronic structure of **1** and also to facilitate interpretation of the experimental data based on the bonding aspects discussed, we have decided to compute the absorption spectra and the spin Hamiltonian parameters for **1**.

TDDFT analysis. The computed absorption spectrum of **1** (Fig. 5) displays a set of d–d bands at 472.6 nm and 588 nm which are in good agreement with the experimental absorption spectrum of **1** where an intense band at 445 nm and weaker and broader band at 660 nm were noted.[61] The intensity of the computed band at 588 nm largely derives from the $\pi_{d_{xz}-p_x}{}^*/\pi_{d_{yz}-p_y}{}^* \rightarrow d_{z^2}$ transition (71%) with a smaller contribution from the π-bonding orbital of $\pi_{d_{yz}-p_y}$ to the respective π-antibonding $\pi_{d_{yz}-p_y}{}^*$ orbital. The higher energy absorption at 472.6 nm arises predominately from $d_{xy} \rightarrow d_{x^2-y^2}$ transition (80%) with some contributions from $d_{xy} \rightarrow \pi_{d_{xz}-p_x}{}^*$ and $d_{xy} \rightarrow d_{z^2}$ transitions. The most intense higher energy band in Fig. 5 at 392 nm is found to be a charge transfer transition. This interpretation correlates also with the energy level diagram supplemented in Fig. 3.

Calculation of spin-Hamiltonian (SH) parameters. The species **1** characterization is complemented with applied-field Mössbauer spectroscopy where hyperfine interaction of ^{57}Fe and axial and rhombic zero-field splitting (ZFS) were estimated.[61] The Mössbauer spectra of **1** is very different from that of **2** where a significant rhombic ZFS were noted for **1** (see Table 4). The computed spin Hamiltonian parameters (tensors g, A, D and Mössbauer spectral parameters) for **1** are summarised in Table 4. The SH parameters were computed for three different spin states $^7\mathbf{1}_{(HS,T)}$, $^5\mathbf{1}_{(HS,S)}$ and $^3\mathbf{1}_{(IS,S)}$ to offer clarity to the experimentally measured values. The computed hyperfine coupling constant for these three spin states implies that the hyperfine interaction is anisotropic in nature. A triplet state has been proposed as the

Table 4 Calculated Mössbauer isomer shift, g, A and D tensor values of $[Fe^{IV}(NTs)(N_4Py)]^{2+}$ along with experimental data

	g_x, g_y, g_z[a]	A_x, A_y, A_z[a]	ΔE_q[b]/mm s^{-1}	η[b]	δ[b]/mm s^{-1}	D[a]/cm^{-1}	E/D[a]
$^7\mathbf{1}_{(HS,T)}$	2.006, 2.009, 2.01	7.9, 15.9, 3.5	0.17	0.23	0.52	−0.98	0.24
$^5\mathbf{1}_{(HS,S)}$	2.009, 2.013, 2.019	−11.1, −17.6, 0.7	1.06	0.84	0.56	4.14	0.26
$^3\mathbf{1}_{(IS,S)}$	1.99, 2.021, 2.035	−15.2, −43.6, 7.2	−0.09	0.30	0.19	4.66	0.22
Exp.	—	−20, −21, −3	+0.98	−0.7	0.02	29	0.23

[a] Computed using B3LYP level. [b] Computed using B86 level.

ground state for **1** only based on the applied-field Mössbauer spectrum where the measured $A_\perp$ values are found to best fit the $S = 1$ state and this is in lieu to the reported $A_\perp$ values of other high-valent $S = 1$ intermediates. On the other hand, a fit with an $S = 2$ state severely underestimate (difference of *ca.* 14 T) the hyperfine tensors measured and thus the possibility of an $S = 2$ ground state is ruled out.[61] It is worth noting here that, the $S = 3$ state has not been considered in the fitting. Calculations reveals that for $^3\mathbf{1}_{(IS,S)}$ species, the predicted $A_\perp/g_n\beta_n$ value is about −29.2 T and this is overestimated by 6.2 T compared to the experimental values.[98] Note here that the $A_\perp/g_n\beta_n$ for other $S = 1$ oxoiron(IV) intermediates falls in the range of −20 to −23 T.[7,99,100] For the $^5\mathbf{1}_{(HS,S)}$ state, the computed $A_\perp/g_n\beta_n$ value is 14.4 T which is in agreement to the experimental $A_\perp/g_n\beta_n$ reported for other $S = 2$ oxoiron(IV) species.[101,102] The value of 14.4 T is much higher than the value 6.5 T estimated from fitting the data collected for **1** assuming an $S = 2$ state. This supports the experimental determination of the ground state of **1** as high spin as it is expected to have larger $A_\perp$ values. Additionally for $^7\mathbf{1}_{(HS,T)}$ the computed $A_\perp/g_n\beta_n$ of 11.9 T is much lower compared to the best fit obtained for $S = 1$ and this reassures that the ground state is $S = 1$ and not $S = 2$ or 3. It is to be noted here that the A_z values are computed to be small for all three spin states.

The Mössbauer spectral parameters were computed using the BP86 functional which is known to predict reasonable estimated MB parameters compared to the experiments.[103] The MB parameters have been previously computed for **1** using the B3LYP functional along with the 6-311G basis set in Gaussian09. Similar to the reported values,[61] the BP86 also yields a large isomer shift (0.19) for the $^3\mathbf{1}_{(IS,S)}$ state compared to the experimental value of 0.02. Besides, the δ computed for $^7\mathbf{1}_{(HS,T)}$ and $^5\mathbf{1}_{(HS,S)}$ spin states are also largely overestimated. The quadruple splitting on the other hand is computed to be very small for $^7\mathbf{1}_{(HS,T)}$ and $^3\mathbf{1}_{(IS,S)}$ spin states while for $^5\mathbf{1}_{(HS,S)}$ a large value is obtained. The calculated asymmetry parameter is about the same in all three spin states. The axial ZFS parameter D is estimated to be small for all three spin states compared to the experiments. However, this is not surprising given the fact that the DFT calculations miss some of the important contributions to the D-tensors and one would require *ab initio* CASSCF or SORCI methods to accurately compute this parameter.[104] The computed rhombic ZFS value of 0.22 is in good agreement with the experimental value and suggests that complex **1** indeed possesses a large rhombic anisotropy. Although the molecular g-tensor values were not determined experimentally (this would require a HF-EPR measurement), we have computed the g-tensor to complement the other data provided here. The computed g-tensor is found to be isotropic in general (see Fig. 2 for g-tensor orientation) and this in good accord to the $S = 1$ g-tensor estimate for the oxoiron(IV) species.[104,105] Although the computed SH parameters deviates from the experimental values in many cases, the relative trend observed remains the same. A more accurate higher level *ab initio* method might be required to obtain good numerical estimates of the SH parameters.

Conclusion

Pure and hybrid DFT methods were used to investigate the structure, energetics and bonding nature of Fe^{IV}═NTs species in comparison with the widely studied Fe^{IV}═O species. The computed results are in general good agreement to the experimental results and in many occasions, it supports and verifies the experimental observations. The conclusions emerging from this work are summarized below,

1. A barrierless cleavage of the N–I bond and a large thermodynamic stability upon forming the Fe^{IV}═NTs species compared to the Fe^{IV}═O complex indicates a facile formation of this intermediate – data consistent with the experimental observation.

2. A method assessment has been undertaken to choose the best functional which can describe the structure and energetics of this species accurately. By testing both the modern and popular functionals, we arrive at the conclusions that the hybrid B3LYP functional marginally behaves better in predicting the correct ground state for Fe^{IV}═NTs species.

3. A detailed bonding analysis reveals many significant interactions in this complex. Notably, due to the presence of a tosyl group on the nitrene nitrogen, the σ-bonding interactions in Fe^{IV}═NTs are found to be weaker than the corresponding bond strength in the Fe^{IV}═O complex. Further the NBO and the EDA tools indicates an ionic Fe^{IV}═NTs and a covalent Fe^{IV}═O bonding scenario in these complexes.

4. The bonding aspects and spin-state energetics were employed to predict the reactivity pattern in Fe^{IV}═NTs species. This analysis reveals that the Fe^{IV}═NTs species are expected to be more reactive than the corresponding Fe^{IV}═O intermediates and the possibility of having an $S = 3$ state for the Fe^{IV}═NTs offers room for further enhancement of reactivity.

5. TD-DFT calculations have been performed to simulate the experimental absorption spectrum. A good agreement between the experiment and theory lead us to interpret the experimental d–d transitions observed.

6. The SH parameters (tensors g, A and D and MB isomer and quadruple splitting) were computed and these parameters help us to assure the ground-state determination for **1** – albeit the fact that many of the computed parameters diverge from the experimental data.

To this end, a comprehensive set of DFT calculations employing energetics-spectroscopic approach utilizing tools such as MO, EDA and NBO analysis has been undertaken to unfold the structure energetics and bonding aspects of a novel Fe^{IV}═NTs species. Further studies on the reactivity Fe^{IV}═NTs species is underway in our laboratory particularly on the aromatic amination reactions.[52]

Computational details

All the geometry optimizations have been performed using the DFT method as implemented in Gaussian 09 program.[106] Unrestricted B3LYP functional with a Los Alamos effective core potential double zeta valence basis set (LANL2DZ)[107,108] on Fe was used and 6-31G(d) basis set was used for C, H, N, O and S atoms and a SDD basis set[109] was employed for iodine atom unless otherwise mentioned. In order to find out which functional is suitable for predicting the spin state energetics and spin densities of different states of **1**, we have tested many functionals and here we restrict ourselves to discuss the outcome of three different functionals B3LYP*,[82,83] M06-2X[84] and BP86[79–81] apart from the B3LYP[82,83] functional and all of which has been shown in many occasions to accurately predict the geometry/spin states of metal complexes. Single-point calculations were performed using the TZVP[110] basis set on the gas-phase optimized geometries in order to improve the energetics computed. All the reported energies are corrected for free energy corrections where frequencies have been computed at the same level that of the geometry optimization. Noodleman's broken symmetry approach[111] has been employed for the purpose of converging the antiferromagnetic-like solutions between Fe and nitrene components. The ORCA package[112] was used to calculate the Mössbauer (MB), UV-Visible spectra and other spin Hamiltonian parameters (g, A and D tensors). Both BP86[79–81] and B3LYP[82,83] exchange correlation functionals were used along with the TZVP basis set on the Gaussian optimized geometries to compute the spectral parameters. MB-Isomer shifts (IS) were calculated based on the calibration constants reported by Römelt *et al.*[113] and 0.16 barn was used for the calculation of quadruple moment of ^{57}Fe. Experimentally, the common way to represent the A-tensor obtained from Mössbauer spectroscopy is in the unit of Tesla and the computed hyperfine from ORCA suite of program is in the unit of MHz from the perspective of EPR spectroscopy. The unit conversion is performed as suggested and here the ground-state nuclear spin conversion factor has been used to convert MHz to Tesla unit.[114] Time dependent density functional theory (TDDFT) implemented in the ORCA program was used for the calculation of excitation energies. The EDA was performed with the BP86 functional and a triple-ζ basis set using ADF program.[90] SCRF-PCM[116] model using B3LYP level have been used to optimized the geometries in solution phase and acetonitrile (CH_3CN) was used as a solvent, and the results are summarized in the ESI.†

Acknowledgements

G. R. would like to acknowledge the financial support from the Government of India through Department of Science and Technology (SR/S1/IC-41/2010) and generous computational resources from Indian Institute of Technology-Bombay. M. J. thanks IIT-Bombay for financial support through Institute Post Doctoral Fellowship. We would like to thank Prof. P. Venuvanalingam, School of Chemistry, Bharathidasan University, Trichy for the EDA analysis using ADF program.

References

1 W. Nam, *Acc. Chem. Res.*, 2007, **40**, 522–531.
2 L. Que, Jr., *Acc. Chem. Res.*, 2007, **40**, 493–500.
3 D. Schroeder, S. Shaik and H. Schwarz, *Acc. Chem. Res.*, 2000, **33**, 139–145.
4 L. Feig and S. J. Lippard, *Chem. Rev.*, 1994, **94**, 759–805.
5 B. Meunier, S. P. de Visser and S. Shaik, *Chem. Rev.*, 2004, **104**, 3947–3980.
6 L. Que, Jr. and R. Y. N. Ho, *Chem. Rev.*, 1996, **96**, 2607–2624.
7 J.-U. Rohde, J.-H. In, M. H. Lim, W. W. Brennessel, M. R. Bukowski, A. Stubna, E. Muenck, W. Nam and L. Que, Jr., *Science*, 2003, **299**, 1037–1039.
8 S. P. de Visser, R. Latifi, L. Tahsini and W.-W. Nam, *Chem.–Asian J.*, 2011, **6**, 493–504.
9 T. A. Jackson, J.-U. Rohde, M. S. Seo, C. V. Sastri, R. DeHont, A. Stubna, T. Ohta, T. Kitagawa, E. Munck, W. Nam and L. Que, *J. Am. Chem. Soc.*, 2008, **130**, 12394–12407.
10 C. V. Sastri, M. J. Park, T. Ohta, T. A. Jackson, A. Stubna, M. S. Seo, J. Lee, J. Kim, T. Kitagawa, E. Munck, L. Que, Jr. and W. Nam, *J. Am. Chem. Soc.*, 2005, **127**, 12494–12495.
11 C. V. Sastri, J. Lee, K. Oh, Y. J. Lee, J. Lee, T. A. Jackson, K. Ray, H. Hirao, W. Shin, J. A. Halfen, J. Kim, L. Que, S. Shaik and W. Nam, *Proc. Natl. Acad. Sci. U. S. A.*, 2007, **104**, 19181–19186.
12 T. Kamachi, T. Kouno, W. Nam and K. Yoshizawa, *J. Inorg. Biochem.*, 2006, **100**, 751–754.
13 D. Kumar, S. P. de Visser and S. Shaik, *J. Am. Chem. Soc.*, 2003, **125**, 13024–13025.
14 C. Esterhuysen and G. Frenking, *Theor. Chem. Acc.*, 2004, **111**, 381–389.
15 D. Kumar, H. Hirao, S. P. de Visser, J. Zheng, D. Wang, W. Thiel and S. Shaik, *J. Phys. Chem. B*, 2005, **109**, 19946–19951.
16 S. Shaik, S. Cohen, Y. Wang, H. Chen, D. Kumar and W. Thiel, *Chem. Rev.*, 2010, **110**, 949–1017.
17 S. Shaik, H. Hirao and D. Kumar, *Acc. Chem. Res.*, 2007, **40**, 532–542.
18 H. Hirao, D. Kumar, W. Thiel and S. Shaik, *J. Am. Chem. Soc.*, 2005, **127**, 13007–13018.
19 S. Shaik, S. P. de Visser, F. Ogliaro, H. Schwarz and D. Schroeder, *Curr. Opin. Chem. Biol.*, 2002, **6**, 556–567.
20 E. J. Klinker, S. Shaik, H. Hirao and L. Que, Jr., *Angew. Chem., Int. Ed.*, 2009, **48**, 1291–1295.
21 H. Hirao, L. Que, Jr., W. Nam and S. Shaik, *Chem.–Eur. J.*, 2008, **14**, 1740–1756.
22 S. Shaik, D. Kumar and S. P. de Visser, *J. Am. Chem. Soc.*, 2008, **130**, 10128–10140.
23 S. Fukuzumi, H. Kotani, T. Suenobu, S. Hong, Y.-M. Lee and W. Nam, *Chem.–Eur. J.*, 2010, **16**, 354–361.
24 H. Chen, W. Lai and S. Shaik, *J. Phys. Chem. Lett.*, 2010, **1**, 1533–1540.
25 S. Shaik, H. Chen and D. Janardanan, *Nat. Chem.*, 2010, **3**, 19–27.
26 S. N. Dhuri, M. S. Seo, Y.-M. Lee, H. Hirao, Y. Wang, W. Nam and S. Shaik, *Angew. Chem., Int. Ed.*, 2008, **47**, 3356–3359.
27 D. Janardanan, Y. Wang, P. Schyman, L. Que, Jr. and S. Shaik, *Angew. Chem., Int. Ed.*, 2010, **49**, 3342–3345.
28 A. Altun, V. Guallar, R. A. Friesner, S. Shaik and W. Thiel, *J. Am. Chem. Soc.*, 2006, **128**, 3924–3925.
29 C. Arunkumar, Y.-M. Lee, J. Y. Lee, S. Fukuzumi and W. Nam, *Chem.–Eur. J.*, 2009, **15**, 11482–11489.
30 P. Comba, M. Maurer and P. Vadivelu, *J. Phys. Chem. A*, 2008, **112**, 13028–13036.
31 P. Comba, M. Maurer and P. Vadivelu, *Inorg. Chem.*, 2009, **48**, 10389–10396.
32 P. Comba and G. Rajaraman, *Inorg. Chem.*, 2008, **47**, 78–93.
33 P. Comba and S. Wunderlich, *Chem.–Eur. J.*, 2010, **16**, 7293–7299.
34 S. P. de Visser, *J. Am. Chem. Soc.*, 2006, **128**, 15809–15818.

35 S. P. de Visser, L. Tahsini and W. Nam, *Chem.–Eur. J.*, 2009, **15**, 5577–5587.
36 C. Hazan, D. Kumar, S. P. de Visser and S. Shaik, *Eur. J. Inorg. Chem.*, 2007, 2966–2974.
37 P. C. Hiberty, C. Megret, L. Song, W. Wu and S. Shaik, *J. Am. Chem. Soc.*, 2006, **128**, 2836–2843.
38 H. Hirao, D. Kumar, L. Que, Jr. and S. Shaik, *J. Am. Chem. Soc.*, 2006, **128**, 8590–8606.
39 M. Jaccob, P. Comba, M. Maurer, P. Vadivelu and P. Venuvanalingam, *Dalton Trans.*, 2011, **40**, 11276–11281.
40 M.-J. Kang, W. J. Song, A.-R. Han, Y. S. Choi, H. G. Jang and W. Nam, *J. Org. Chem.*, 2007, **72**, 6301–6304.
41 S. O. Kim, C. V. Sastri, M. S. Seo, J. Kim and W. Nam, *J. Am. Chem. Soc.*, 2005, **127**, 4178–4179.
42 D. Kumar, S. P. de Visser, P. K. Sharma, H. Hirao and S. Shaik, *Biochemistry*, 2005, **44**, 8148–8158.
43 D. Kumar, E. Derat, A. M. Khenkin, R. Neumann and S. Shaik, *J. Am. Chem. Soc.*, 2005, **127**, 17712–17718.
44 W. Nam, S. W. Jin, M. H. Lim, J. Y. Ryu and C. Kim, *Inorg. Chem.*, 2002, **41**, 3647–3652.
45 D. Kumar, S. P. de Visser and S. Shaik, *Chem.–Eur. J.*, 2005, **11**, 2825–2835.
46 S. P. de Visser, K. Oh, A.-R. Han and W. Nam, *Inorg. Chem.*, 2007, **46**, 4632–4641.
47 S. Hong, Y.-M. Lee, K.-B. Cho, K. Sundaravel, J. Cho, M. J. Kim, W. Shin and W. Nam, *J. Am. Chem. Soc.*, 2011, **133**, 11876–11879.
48 D. Kumar, S. P. de Visser and S. Shaik, *J. Am. Chem. Soc.*, 2003, **125**, 13024–13025.
49 H. Chen, K.-B. Cho, W. Lai, W. Nam and S. Shaik, *J. Chem. Theory Comput.*, 2012, **8**, 915–926.
50 Y. Suh, M. S. Seo, K. M. Kim, Y. S. Kim, H. G. Jang, T. Tosha, T. Kitagawa, J. Kim and W. Nam, *J. Inorg. Biochem.*, 2006, **100**, 627–633.
51 D. Janardanan, D. Usharani, H. Chen and S. Shaik, *J. Phys. Chem. Lett.*, 2011, **2**, 2610–2617.
52 M. P. Jensen, M. P. Mehn and L. Que, Jr., *Angew. Chem., Int. Ed.*, 2003, **42**, 4357–4360.
53 Y. Moreau, H. Chen, E. Derat, H. Hirao, C. Bolm and S. Shaik, *J. Phys. Chem. B*, 2007, **111**, 10288–10299.
54 C. A. Grapperhaus, B. Mienert, E. Bill, T. Weyhermueller and K. Wieghardt, *Inorg. Chem.*, 2000, **39**, 5306–5317.
55 M. P. Mehn and J. C. Peters, *J. Inorg. Biochem.*, 2006, **100**, 634–643.
56 J. J. Scepaniak, R. P. Bontchev, D. L. Johnson and J. M. Smith, *Angew. Chem., Int. Ed.*, 2011, **50**, 6630–6633.
57 J. J. Scepaniak, M. D. Fulton, R. P. Bontchev, E. N. Duesler, M. L. Kirk and J. M. Smith, *J. Am. Chem. Soc.*, 2008, **130**, 10515–10517.
58 J. J. Scepaniak, C. G. Margarit, J. N. Harvey and J. M. Smith, *Inorg. Chem.*, 2011, **50**, 9508–9517.
59 R. L. Lucas, D. R. Powell and A. S. Borovik, *J. Am. Chem. Soc.*, 2005, **127**, 11596–11597.
60 R. E. Cowley, N. A. Eckert, S. Vaddadi, T. M. Figg, T. R. Cundari and P. L. Holland, *J. Am. Chem. Soc.*, 2011, **133**, 9796–9811.
61 E. J. Klinker, T. A. Jackson, M. P. Jensen, A. Stubna, G. Juhasz, E. L. Bominaar, E. Muenck and L. Que, Jr., *Angew. Chem., Int. Ed.*, 2006, **45**, 7394–7397.
62 (*a*) D. Kumar, H. Hirao, L. Que, Jr. and S. Shaik, *J. Am. Chem. Soc.*, 2005, **127**, 8026–8027; (*b*) J. Kaizer, E. J. Klinker, N. Y. Oh, J.-U. Rohde, W. J. Song, A. Stubna, J. Kim, E. Münck, W. Nam and L. Que Jr., *J. Am. Chem. Soc.*, 2004, **126**, 472–473.
63 R. Silaghi-Dumitrescu, *Rev. Chim. (Bucharest, Rom.)*, 2007, **58**, 461–464.
64 A. Decker, J. U. Rohde, L. Que, Jr. and E. I. Solomon, *J. Am. Chem. Soc.*, 2004, **126**, 5378–5379.
65 A. Decker, J.-U. Rohde, E. J. Klinker, S. D. Wong, L. Que, Jr. and E. I. Solomon, *J. Am. Chem. Soc.*, 2007, **129**, 15983–15996.
66 S. J. Kim, R. Latifi, H. Y. Kang, W. Nam and S. P. de Visser, *Chem. Commun.*, 2009, 1562–1564.
67 K.-B. Cho, Y. Moreau, D. Kumar, D. A. Rock, J. P. Jones and S. Shaik, *Chem.–Eur. J.*, 2007, **13**, 4103–4115.
68 J. S. McConaghy and W. Lwowski, *J. Am. Chem. Soc.*, 1967, **89**, 2357–2364.
69 P. S. Drzaic and J. I. Brauman, *J. Am. Chem. Soc.*, 1984, **106**, 3443–3446.
70 G. Smolinsky, E. Wasserman and W. A. Yager, *J. Am. Chem. Soc.*, 1962, **84**, 3220–3221.
71 E. Wasserman, G. Smolinsky and W. A. Yager, *J. Am. Chem. Soc.*, 1964, **86**, 3166–3167.
72 P. Brandt, M. J. SÃdergren, P. G. Andersson and P.-O. Norrby, *J. Am. Chem. Soc.*, 2000, **122**, 8013–8020.
73 P. Comba, C. Lang, d. L. C. Lopez, A. Muruganantham, G. Rajaraman, H. Wadepohl and M. Zajaczkowski, *Chem.–Eur. J.*, 2008, **14**, 5313–5328.
74 Y. J. Jeong, Y. Kang, A.-R. Han, Y.-M. Lee, H. Kotani, S. Fukuzumi and W. Nam, *Angew. Chem., Int. Ed.*, 2008, **47**, 7321–7324.
75 E. D. Glendening, K. Badenhoop, A. E. Reed, J. E. Carpenter, J. A. Bohmann, C. M. Morales and F. Weinhold, *NBO 5.0*, Theoretical Chemistry Institute, University of Wisconsin, Madison, 2001.
76 K. Morokuma, *J. Chem. Phys.*, 1971, **55**, 1236–1244.
77 M. V. Hopffgarten and G. Frenking, *Wiley Interdiscip. Rev.: Comput. Mol. Sci.*, 2012, **2**, 43–62.
78 T. Ziegler and A. Rauk, *Theor. Chem. Acc.*, 1977, **46**, 1–10.
79 J. P. Perdew, *Phys. Rev. B*, 1986, **33**, 8822–8824.
80 J. P. Perdew and W. Yue, *Phys. Rev. B*, 1986, **33**, 8800–8802.
81 D. Becke, *Phys. Rev.*, 1988, 3098–3100.
82 C. Lee, W. Yang and R. G. Parr, *Phys. Rev. B*, 1988, **37**, 785–789.
83 D. Becke, *J. Chem. Phys.*, 1993, **98**, 5648–5652.
84 Y. Zhao and D. G. Truhlar, *J. Chem. Phys.*, 2006, **125**, 194101–194118; Y. Zhao and D. Truhlar, *Theor. Chem. Acc.*, 2007, **120**, 215–241.
85 T. Borowski, V. Georgiev and P. E. M. Siegbahn, *J. Mol. Model.*, 2010, **16**, 1673–1677; T. Borowski, T. Bassan, N. G. J. Richards and P. E. M. Siegbahn, *J. Chem. Theory Comput.*, 2005, **1**, 686–693.
86 R. Valero, R. Costa, I. d. P. R. Moreira, D. G. Truhlar and F. Illas, *J. Chem. Phys.*, 2008, **128**, 114103–114108.
87 Y. Morimoto, H. Kotani, J.-Y. Park, Y.-M. Lee, W.-W. Nam and S.-I. Fukuzumi, *J. Am. Chem. Soc.*, 2011, **133**, 403–405.
88 S. Fukuzumi, Y. Morimoto, H. Kotani, P. E. Naumov, Y.-M. Lee and W. Nam, *Nat. Chem.*, 2010, **2**, 756–759.
89 F. F. Pfaff, S. Kundu, M. Risch, S. Pandian, F. Heims, I. Pryjomska-Ray, P. Haack, R. Metzinger, E. Bill, H. Dau, P. Comba and K. Ray, *Angew. Chem., Int. Ed.*, 2011, **50**, 1711–1715.
90 E. J. Baerends, *ADF2008.01*, SCM, Theoretical Chemistry, Vrije Universiteit, Amsterdam, The Netherlands, Scientific Computing & Modelling NV, Amsterdam, The Netherlands, 2008.
91 G. Frenking and N. Froehlich, *Chem. Rev.*, 2000, **100**, 717–774.
92 G. Frenking and A. Krapp, *J. Comput. Chem.*, 2007, **28**, 15–24.
93 G. te Velde, F. M. Bickelhaupt, E. J. Baerends, C. Fonseca Guerra, S. J. A. van Gisbergen, J. G. Snijders and T. Ziegler, *J. Comput. Chem.*, 2001, **22**, 931–967.
94 A. Decker and E. I. Solomon, *Angew. Chem., Int. Ed.*, 2005, **44**, 2252–2255.
95 S. Shaik, D. Kumar, S. P. de Visser, A. Altun and W. Thiel, *Chem. Rev.*, 2005, **105**, 2279–2328.
96 D. J. Fox and R. G. Bergman, *J. Am. Chem. Soc.*, 2003, **125**, 8984–8985.
97 D. J. Fox and R. G. Bergman, *Organometallics*, 2004, **23**, 1656–1670.
98 Note: See Table 4 for individual values; $A_{\perp}$ is calculated as $(A_x + A_y)/2$.
99 M. R. Bukowski, K. D. Koehntop, A. Stubna, E. L. Bominaar, J. A. Halfen, E. Munck, W. Nam and L. Que, *Science*, 2005, **310**, 1000–1002.
100 M. H. Lim, J.-U. Rohde, A. Stubna, M. R. Bukowski, M. Costas, R. Y. N. Ho, E. Munck, W. Nam and L. Que, Jr., *Proc. Natl. Acad. Sci. U. S. A.*, 2003, **100**, 3665–3670.
101 K. L. Kostka, B. G. Fox, M. P. Hendrich, T. J. Collins, C. E. F. Rickard, L. J. Wright and E. Munck, *J. Am. Chem. Soc.*, 1993, **115**, 6746–6757.
102 J. C. Price, E. W. Barr, B. Tirupati, J. M. Bollinger and C. Krebs, *Biochemistry*, 2003, **42**, 7497–7508.
103 M. S. M. Radoul, A. Potapov, C. Riplinger, F. Neese and D. Goldfarb, *Phys. Chem. Chem. Phys.*, 2010, **12**, 7276–7289.
104 D. G. M. Atanasov, D. A. Pantazis, K. Sivalingam and F. Neese, *Inorg. Chem.*, 2011, **50**, 7460.
105 E. B. F. Berry, E. Bothe, F. Neese and K. Wieghardt, *J. Am. Chem. Soc.*, 2006, **128**, 13515–13528.
106 M. J. Frisch, G. W. Trucks, H. B. Schlegel, G. E. Scuseria, M. A. Robb, J. R. Cheeseman, G. Scalmani, V. Barone, B. Mennucci, G. A. Petersson, H. Nakatsuji, M. Caricato, X. Li, H. P. Hratchian, A. F. Izmaylov, J. Bloino, G. Zheng, J. L. Sonnenberg, M. Hada, M. Ehara, K. Toyota, R. Fukuda, J. Hasegawa, M. Ishida, T. Nakajima, Y. Honda, O. Kitao, H. Nakai, T. Vreven, J. A. Montgomery, Jr., J. E. Peralta, F. Ogliaro, M. Bearpark, J. J. Heyd, E. Brothers, K. N. Kudin, V. N. Staroverov, R. Kobayashi, J. Normand, K. Raghavachari, A. Rendell, J. C. Burant, S. S. Iyengar, J. Tomasi, M. Cossi, N. Rega, J. M. Millam, M. Klene, J. E. Knox, J. B. Cross,

V. Bakken, C. Adamo, J. Jaramillo, R. Gomperts, R. E. Stratmann, O. Yazyev, A. J. Austin, R. Cammi, C. Pomelli, J. Ochterski, R. L. Martin, K. Morokuma, V. G. Zakrzewski, G. A. Voth, P. Salvador, J. J. Dannenberg, S. Dapprich, A. D. Daniels, O. Farkas, J. B. Foresman, J. V. Ortiz, J. Cioslowski and D. J. Fox, *GAUSSIAN 09 (Revision A.1)*, Gaussian, Inc., Wallingford, CT, 2009.
107 P. J. Hay and W. R. Wadt, *J. Chem. Phys.*, 1985, **82**, 299–310.
108 W. R. Wadt and P. J. Hay, *J. Chem. Phys.*, 1985, **82**, 284–298.
109 W. Kãchle, M. Dolg, H. Stoll and H. Preuss, *Mol. Phys.*, 1991, **74**, 1245–1263.
110 W. J. Stevens, M. Krauss, H. Basch and P. G. Jasien, *Can. J. Chem.*, 1992, **70**, 612–630.
111 L. Noodleman, *J. Chem. Phys.*, 1981, **74**, 5737–5743.
112 F. Neese, *Density Functional and Semiempirical Program Package, version 2.8*, University of Bonn, Bonn, Germany, 2009.
113 M. Romelt, S. Ye and F. Neese, *Inorg. Chem.*, 2009, **48**, 784–785.
114 E. B. P. Gütlich and A. X. Trautwein, *Mössbauer Spectroscopy and Transition Metal Chemistry: Fundamentals and Applications*, Springer, Berlin, 2011, pp. 553–555.
115 Note: It is to be noted here that as we are interested in understanding the relative strength of Fe–X bonding in **1** and **2**, the computed frequencies were not scaled and thus the absolute values differ from the experimentally reported values.
116 S. Miertus, E. Scrocco and J. Tomasi, *Chem. Phys.*, 1981, **55**, 117–129.